AGU PUBLICATIONS

Geophysical Research Letters

RESEARCH LETTER

10.1002/2014GL062444

Key Points:
- Aerosol optical extinction in the southeastern U.S. is dominated by scattering
- Black carbon is a more significant absorber than organic carbon at 365 nm
- Biomass burning makes the largest contribution to organic aerosol absorption

Supporting Information:
- Readme
- Texts S1 and S2, Tables S1 and S2, and Figures S1 and S2

Correspondence to:
R. A. Washenfelder,
rebecca.washenfelder@noaa.gov

Citation:
Washenfelder, R. A., et al. (2015), Biomass burning dominates brown carbon absorption in the rural southeastern United States, *Geophys. Res. Lett.*, *42*, doi:10.1002/2014GL062444.

Received 11 NOV 2014
Accepted 29 DEC 2014
Accepted article online 7 JAN 2015

Biomass burning dominates brown carbon absorption in the rural southeastern United States

R. A. Washenfelder[1,2], A. R. Attwood[1,2,3], C. A. Brock[2], H. Guo[4], L. Xu[5], R. J. Weber[4], N. L. Ng[4,5], H. M. Allen[6,7], B. R. Ayres[6], K. Baumann[8], R. C. Cohen[9,10], D. C. Draper[6,11], K. C. Duffey[10], E. Edgerton[8], J. L. Fry[6], W. W. Hu[1,12], J. L. Jimenez[1,12], B. B. Palm[1,12], P. Romer[10], E. A. Stone[13], P. J. Wooldridge[10], and S. S. Brown[1,2]

[1]Cooperative Institute for Research in Environmental Sciences, University of Colorado Boulder, Boulder, Colorado, USA, [2]Chemical Sciences Division, Earth System Research Laboratory, National Oceanic and Atmospheric Administration, Boulder, Colorado, USA, [3]Now at Horiba Scientific, Edison, New Jersey, USA, [4]School of Earth and Atmospheric Sciences, Georgia Institute of Technology, Atlanta, Georgia, USA, [5]School of Chemical and Biomolecular Engineering, Georgia Institute of Technology, Atlanta, Georgia, USA, [6]Department of Chemistry, Reed College, Portland, Oregon, USA, [7]Now at Division of Chemistry and Chemical Engineering, California Institute of Technology, Pasadena, California, USA, [8]Atmospheric Research & Analysis, Inc., Cary, North Carolina, USA, [9]Department of Earth and Planetary Science, University of California, Berkeley, California, USA, [10]Department of Chemistry, University of California, Berkeley, California, USA, [11]Now at Department of Chemistry, University of California, Irvine, California, USA, [12]Department of Chemistry and Biochemistry, University of Colorado Boulder, Boulder, Colorado, USA, [13]Department of Chemistry, University of Iowa, Iowa City, Iowa, USA

Abstract Brown carbon aerosol consists of light-absorbing organic particulate matter with wavelength-dependent absorption. Aerosol optical extinction, absorption, size distributions, and chemical composition were measured in rural Alabama during summer 2013. The field site was well located to examine sources of brown carbon aerosol, with influence by high biogenic organic aerosol concentrations, pollution from two nearby cities, and biomass burning aerosol. We report the optical closure between measured dry aerosol extinction at 365 nm and calculated extinction from composition and size distribution, showing agreement within experiment uncertainties. We find that aerosol optical extinction is dominated by scattering, with single-scattering albedo values of 0.94 ± 0.02. Black carbon aerosol accounts for $91 \pm 9\%$ of the total carbonaceous aerosol absorption at 365 nm, while organic aerosol accounts for $9 \pm 9\%$. The majority of brown carbon aerosol mass is associated with biomass burning, with smaller contributions from biogenically derived secondary organic aerosol.

1. Introduction

Absorption and scattering of light by aerosol play an important role in the Earth's radiative budget [*Solomon et al.*, 2007]. The three identified types of light-absorbing aerosol are black carbon, mineral dust, and brown carbon. Brown carbon aerosol is defined as light-absorbing organic particulate matter with wavelength-dependent absorption, determined to vary as λ^{-2}–λ^{-6}, where λ is the wavelength of light in nm [*Andreae and Gelencsér*, 2006]. Calculations using aerosol optical depth have determined that the contribution of brown carbon to total carbonaceous aerosol absorption is 28% at 440 nm in California [*Bahadur et al.*, 2012] and 20% at 550 nm globally [*Chung et al.*, 2012]. Because the absorption increases at short wavelengths, the radiative effects of brown carbon aerosol are greatest in the ultraviolet spectral region.

Both primary and secondary sources of brown carbon aerosol have been identified, including combustion of fossil fuels [*Bond*, 2001], biomass burning [*Kirchstetter et al.*, 2004; *Lack et al.*, 2012], biological aerosols (e.g., soil humics and bioaerosols) [*Andreae and Crutzen*, 1997], and secondary organic aerosol formed from anthropogenic or biogenic precursors (see references below). While the primary brown carbon sources are straightforward to identify, mechanisms to produce light-absorbing secondary organic aerosol are not confirmed. Proposed mechanisms include nitration of polycyclic aromatic hydrocarbons to yield light-absorbing nitrophenols [*Pitts et al.*, 1978; *Jacobson*, 1999]; reaction of NH_3, NH_4^+, or amino acids with condensed-phase carbonyl products [*Bones et al.*, 2010; *Sareen et al.*, 2010; *Updyke et al.*, 2012; *Flores et al.*, 2014]; acid-catalyzed aldol condensation of volatile aldehydes [*Noziere and Esteve*, 2005, 2007]; reaction of OH radicals with aromatic hydroxyacids and phenols in cloud water [*Gelencser et al.*, 2003; *Hoffer et al.*, 2004]; heterogeneous

©2015. American Geophysical Union. All Rights Reserved.

reactions of isoprene on acidic aerosol particles [*Limbeck et al*., 2003]; aqueous photochemistry of pyruvic acid in the presence of atmospheric electrolytes (e.g., SO_4^{2-} and NH_4^+) [*Rincon et al*., 2009, 2010]; and reaction of isoprene epoxydiols onto sulfate aerosol to form absorbing oligomers [*Lin et al*., 2014]. Few field measurements have been able to link these mechanisms and products directly to brown carbon aerosol [*Zhang et al*., 2011; *Mohr et al*., 2013; *Lin et al*., 2014].

In this work, we analyze anthropogenic, biomass burning, and biogenic secondary organic aerosol as potential contributors to brown carbon in the southeastern U.S. Measurements were conducted during June–July 2013 in the Talladega National Forest in central Alabama. The primary goal of the campaign was to examine the influence of anthropogenic emissions in a region with very large biogenic emissions. The site is well located to examine sources of brown carbon aerosol because it is influenced by high biogenic organic aerosol concentrations, two nearby cities, and biomass burning aerosol.

The field site contained a large suite of instruments to measure aerosol optical properties and composition, including broadband cavity-enhanced spectroscopy (BBCES) [*Fiedler et al*., 2003; *Washenfelder et al*., 2013] and UV/visible absorption spectra of water-soluble organic carbon (WSOC) [*Hecobian et al*., 2010; *Zhang et al*., 2013]. We use aerosol optical property measurements, along with measurements of aerosol composition and size distribution, to examine (1) the optical closure between measured dry aerosol extinction and calculated dry aerosol extinction from composition and size distribution; (2) the magnitude of brown and black carbon absorption; (3) the relative contributions of biomass burning, anthropogenic, and secondary organic aerosol to brown carbon absorption in the southeastern U.S. during summer.

2. Experiment

2.1. Overview of the SOAS Field Site in Central Alabama

The Southern Oxidant and Aerosol Study (SOAS) ground site was located in the Talladega National Forest in central Alabama (32.90328°N, 87.24994°W, 76.5 m above mean sea level). It was colocated with the Electric Power Research Institute Southeastern Aerosol Research and Characterization Network (SEARCH) Centreville site, which includes ongoing measurements of gas-phase pollutants, aerosol composition, nephelometry, and meteorology [*Hansen et al*., 2003; *Edgerton et al*., 2005, 2006]. The site is approximately 42 km southeast of Tuscaloosa (population 90,468) and 76 km southwest of Birmingham (population 212,237), and is heavily forested with pine (loblolly, shortleaf, longleaf, and slash) and hardwoods. The Model of Emissions of Gases and Aerosols from Nature (MEGAN) shows that isoprene emissions from the site are representative of the southeastern U.S. and among the highest in the world [*Guenther et al*., 2012]. Observed wind directions during the SOAS field campaign were variable and included periods of urban influence from Tuscaloosa and Birmingham. A map of the field site and a wind rose are included in the supporting information.

2.2. Aerosol Optical Extinction Instruments

In this analysis, we use measurements of aerosol optical extinction by BBCES, scattering by nephelometry, and WSOC absorption by UV/visible (VIS)-particle-into-liquid sampler (PILS). The measurements are described briefly below. Full details are given in the supporting information.

2.2.1. Broadband Cavity-Enhanced Spectroscopy (BBCES)

Broadband cavity-enhanced spectroscopy (BBCES) has been used to measure gas-phase absorbers [*Fiedler et al*., 2003; *Ball et al*., 2004; *Venables et al*., 2006] and broadband aerosol extinction [*Washenfelder et al*., 2008; *Varma et al*., 2009; *Thalman and Volkamer*, 2010; *Varma et al*., 2013; *Washenfelder et al*., 2013]. BBCES employs a broadband light source, high-finesse cavity, and multichannel detector to make continuous, real-time, in situ measurements of extinction over a broad spectral region. In the laboratory, it has been used with size-selected measurements and Mie theory to retrieve complex refractive indices as a function of wavelength for both standard aerosol samples [*Washenfelder et al*., 2013] and aged secondary organic aerosol [*Flores et al*., 2014]. Aerosol concentrations were too low during the SOAS field campaign for this method, which requires size-selected aerosol concentrations greater than 10 particles cm^{-3}, so total extinction was measured as a function of wavelength. In situ aerosol optical extinction at 355–420 nm was measured continuously using a field instrument with three optical cavities. This is a modified version of the field instrument previously used to measure CHOCHO, HONO, and NO_2 [*Washenfelder et al*., 2011, 2013].

©2015. American Geophysical Union. All Rights Reserved.

Table 1. Aerosol Composition Measurements at the SOAS 2013 Ground Site Used in This Analysis

Species	Technique	Size Cut (μm)	Acquisition Time	Reference
Total OA, BBOA, LO-OOA, MO-OOA, Isoprene-OA	Aerosol mass spectrometer (AMS) positive matrix factorization (PMF)	1.0	5 h^{-1}	*DeCarlo et al.* [2006]
Water-soluble organic carbon	Particle-into-liquid sampler (PILS)	2.5	6 min	*Hecobian et al.* [2010]
Black carbon	Multiangle absorption photometry (MAAP)	2.5	10 min	*Petzold et al.* [2002]
NH_4^+, Na^+, Ca^{2+}, NO_3^-, SO_4^{2-}	Monitor for Aerosols and Gases in Ambient Air (MARGA)	2.5	1 h	*Rumsey et al.* [2014]
Si, Ti, Ca, Fe, Al	X-ray fluorescence (XRF)	2.5	24 h	*Edgerton et al.* [2005]
Levoglucosan	Solvent extraction gas chromatography-mass spectrometry	2.5	11 h	*Nolte et al.* [2002]
Alkyl nitrate	Thermal decomposition - laser induced fluorescence (TD-LIF)	2.5	1 min	*Rollins et al.* [2010]
$PM_{2.5}$ aerosol mass	Tapered element oscillating microbalance (TEOM)	2.5	5 min	*Edgerton et al.* [2006]

The inlet flow was conditioned prior to entering the cavities using two nafion dryers in parallel (RH $<$ 10%; PP-110-12-MSS, Perma Pure, Toms River, NJ), an inertial impactor with a 50% cut point at an aerosol aerodynamic diameter of 2.5 μm (TE296, Tisch Environmental, Cleves, OH), and an activated carbon denuder. The denuder removed NO_2 and HONO, which have structured absorption in the UV spectral region, with efficiency $>$99.5% for NO_2 and $>$90% for HONO during laboratory tests. The uncertainty in the BBCES aerosol extinction is 4% and includes uncertainty in the Rayleigh scattering cross sections for N_2 and O_2, sample pressure, sample temperature, sample and mirror purge flows, and particle losses [*Washenfelder et al.*, 2013].

2.2.2. UV/Visible Absorption of Water-Soluble Organic Carbon

Absorption spectra of water soluble $PM_{2.5}$ aerosol components were measured semicontinuously using a particle-into-liquid sampler (PILS) coupled in series with a long optical path length (2.5 m) liquid waveguide capillary cell (LWCC; World Precision Instrument, Sarasota, FL) and a total organic carbon (TOC) analyzer (GE Analytical, Boulder, CO) [*Hecobian et al.*, 2010; *Liu et al.*, 2013; *Zhang et al.*, 2013]. Complete light absorption spectra between wavelengths of 200 and 800 nm of the $PM_{2.5}$ aqueous extracts were recorded with a UV/visible spectrometer (Ocean Optics, Dunedin, FL) at a time resolution of 15 min. The PILS-LWCC-TOC instrument provides a direct measurement of the water-soluble portion of brown carbon absorption, which is not available from other aerosol optical instruments.

The measurement uncertainties of the WSOC absorption and WSOC mass were 30% and 8%, respectively. Prior studies have consistently shown that light absorption by organic carbon extracted in methanol is larger than for water extracts [*Chen and Bond*, 2010; *Liu et al.*, 2013]. We have calculated the organic aerosol (OA) absorption by multiplying the WSOC absorption by 1.43 ± 0.31, which was determined from UV/visible absorption spectra of $PM_{2.5}$ filter samples collected at the SOAS field site during June 2013. Methanol extractions were performed after water extractions for the same filters, so the scaling is an exact correction. During SOAS 2013, the average ratio of water-soluble organic aerosol (WSOA) mass to total OA was 0.89 ± 0.21, which was determined from an aerosol mass spectrometer (AMS) measurement of WSOA using a PILS and the AMS measurement of total ambient OA mass described below. We assume that the PILS-LWCC-TOC absorption measurement multiplied by 1.43 is representative of the total OA mass.

2.2.3. Nephelometer

Aerosol scattering was measured using an integrating nephelometer at 530 nm (M903, Radiance Research, Seattle, WA, USA), with continuous sampling at 5 min intervals [*Edgerton et al.*, 2006]. The ambient sample was dried with a Nafion dryer, and a 2.5 μm dry size cut was applied. The measurement was corrected for Rayleigh scattering based on the internal temperature and pressure of the nephelometer.

2.3. Aerosol Composition Measurements

Table 1 summarizes the aerosol composition measurements used for this analysis, including black carbon mass by multiangle absorption photometry (MAAP; Model 5012, Thermo Scientific, Waltham, MA, USA); WSOC (PILS) [*Hecobian et al.*, 2010]; soluble ions by a stream jet aerosol collector and ion chromatography (Monitor for Aerosols and Gases in Ambient Air; MARGA) [*Slanina et al.*, 2001; *Rumsey et al.*, 2014]; insoluble minerals by X-ray fluorescence [*Edgerton et al.*, 2005]; levoglucosan by Soxhlet extraction into dichloromethane and acetone with silylation derivatization at 70°C in pyridine for detection by gas chromatography-mass spectrometry [*Nolte et al.*, 2002]; and total $PM_{2.5}$ aerosol mass measured by tapered element oscillating microbalance (TEOM) [*Edgerton et al.*, 2006].

©2015. American Geophysical Union. All Rights Reserved.

The composition of submicron nonrefractory aerosol was measured by a high-resolution time-of-flight aerosol mass spectrometer (HR-ToF-AMS, Aerodyne Research Inc., Billerica, MA, USA), which has been described previously [*DeCarlo et al*., 2006; *Canagaratna et al*., 2007]. Details on the HR-ToF-AMS operation and data processing during SOAS can be found in *Xu et al*. [2014] and the supporting information. Briefly, positive matrix factorization (PMF) analysis was performed on the time series of high-resolution organic aerosol mass spectra [*Ulbrich et al*., 2009] to resolve four organic aerosol (OA) subtypes: more-oxidized oxygenated OA (MO-OOA), less-oxidized oxygenated OA (LO-OOA), biomass burning OA (BBOA), and isoprene-derived OA (Isoprene-OA), which account for 39%, 32%, 10%, and 18% of total organic mass on average [*Xu et al*., 2014]. MO-OOA had the highest atomic O:C ratio (0.8) and likely represents highly aged OA from multiple sources. LO-OOA (O:C = 0.46), which reaches a daily maximum at night and correlates with particle-phase organic nitrates, has a substantial contribution from nighttime reactions between monoterpenes and NO_3 radical [*Xu et al*., 2014]. The BBOA factor has a prominent signal for ions likely associated with levoglucosan (*m/z* 60 ($C_2H_4O_2^+$) and *m/z* 73 ($C_3H_5O_2^+$)) and is correlated with levoglucosan measured in $PM_{2.5}$ filter samples ($r^2 = 0.57$). The Isoprene-OA factor is mainly linked to secondary organic aerosol (SOA) from the reactive uptake of isoprene epoxydiols in the presence of hydrated sulfate.

Aerosol alkyl nitrate was measured by thermal decomposition to $RO + NO_2$, followed by detection of NO_2 with laser-induced fluorescence (TD-LIF) [*Rollins et al*., 2010]. Gas-phase NO_2 and nitrates (RO_2NO_2 and $RONO_2$) were removed from the sample stream with an activated carbon denuder [*Rollins et al*., 2010]. Because the molecular composition of the alkyl nitrate species is unknown, the aerosol mass concentration was calculated using a molecular mass of 250 g mol^{-1}, which is within the range of 200–300 g mol^{-1} for the expected condensed species.

2.4. Additional Data Sets

Aerosol size distribution was measured by a scanning mobility particle sizer for 13–710 nm diameter (3080 Electrostatic Classifier, 3081 Differential Mobility Analyzer, and 3010 CPC; TSI Inc., Shoreview, MN, USA) and an optical particle counter for 710–4000 nm diameter (GRIMM Aerosol Technik GmbH, Ainring, Germany). Gas-phase species, including CO, and meteorological parameters, including wind speed and direction, were monitored continuously at the Centreville SEARCH site [*Hansen et al*., 2003].

3. Results and Discussion

3.1. Optical Closure Between Measured and Calculated Extinction

Figure 1a shows dry aerosol extinction measured at 360, 405, and 420 nm by the BBCES instrument, along with the dry aerosol scattering at 530 nm. The extinction values varied between 10 and 200 Mm^{-1}. The highest extinction values were observed during a biomass burning event on 4 June 2013. The lowest extinction values were observed during a period of heavy rain on 4–7 July 2013.

We compare the measured extinction to an independently calculated extinction value determined from Mie theory using aerosol size distributions and volume-weighted refractive indices determined from composition. The major components of the aerosol mass composition are shown in Figure 1b. A complete list of the aerosol mass components is given in the supporting information (Table S2). MARGA measurements of NH_4^+, Na^+, Cl^-, NO_3^-, SO_4^{2-} mass concentrations have been assigned to electrolytes using the extended Aerosol Inorganics Model III [*Clegg et al*., 1998]. The Si, Al, Ca, Fe, and Ti concentrations measured by XRF are assigned as SiO_2, Al_2O_3, CaO, Fe_2O_3, and TiO_2. The organic aerosol mass is determined by AMS. The two dominant components of aerosol mass in the southeastern U.S. are organic and partially neutralized sulfate [*Edgerton et al*., 2005], as shown in Figure 1b. An orthogonal distance regression fit between the sum of the aerosol mass components and the TEOM $PM_{2.5}$ mass has an intercept of 1.2 ± 0.2 ug m^{-3} and a slope of 1.03 ± 0.02, indicating that the sum correctly represents the majority of the $PM_{2.5}$ aerosol mass.

Volume-weighted refractive indices, $\overline{m}$ (where $m = n + ki$), are shown in Figure 1c, calculated according to [*Ouimette and Flagan*, 1982]:

$$\overline{m} = \overline{\rho} \sum_i \frac{c_i m_i}{\rho_i} \tag{1}$$

where ρ is density and c_i is the mass fraction of component *i*. Densities and refractive indices for the inorganic components are given in the supporting information (Table S2). Values for black carbon were taken from

©2015. American Geophysical Union. All Rights Reserved.

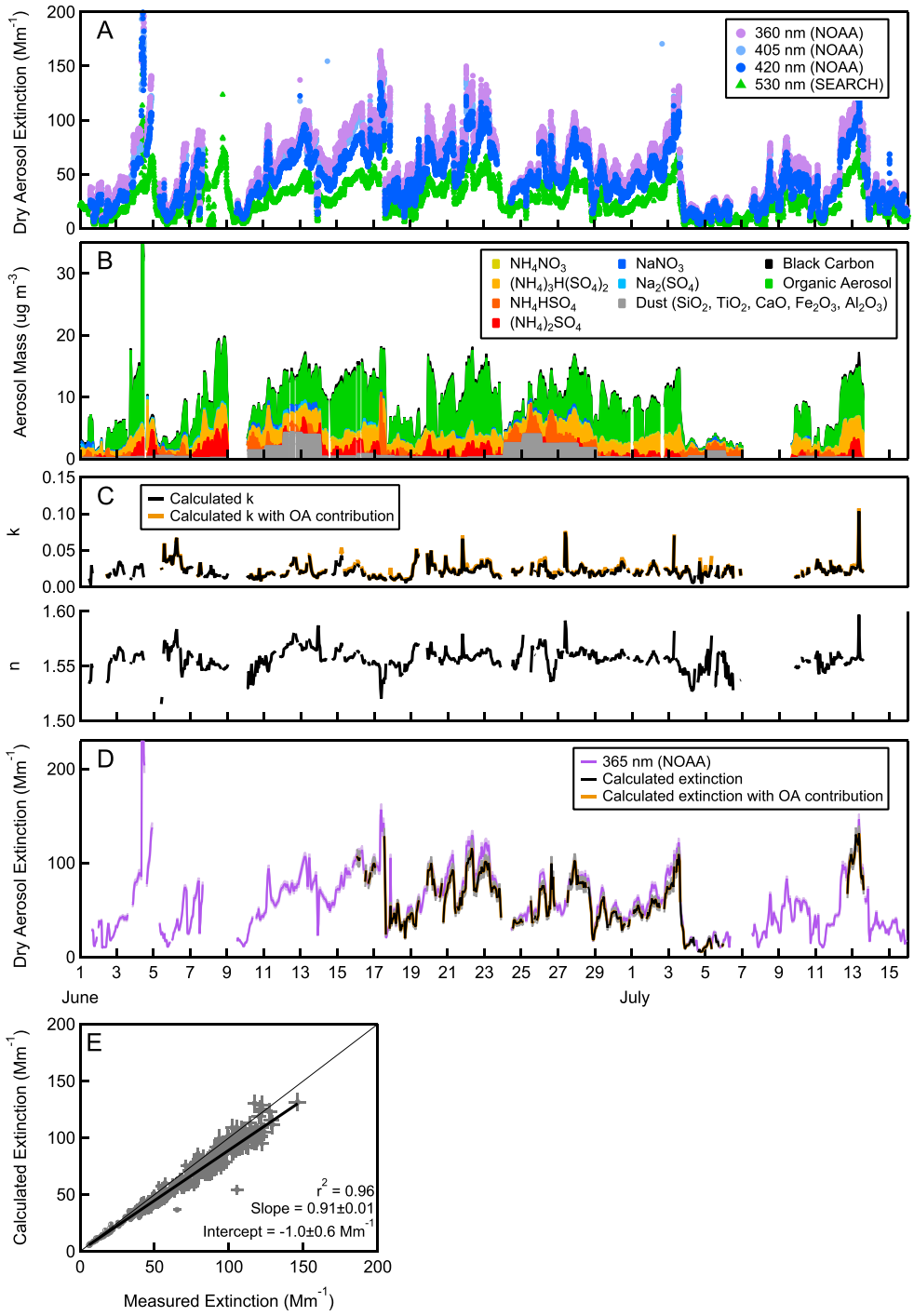

Figure 1. (a) Dry aerosol extinction measured by the NOAA BBCES (360, 405, and 420 nm) and dry aerosol scattering measured by nephelometry (530 nm). (b) Aerosol mass measured by MARGA with inorganic ions assigned to salts using the Aerosol Inorganics Model III [*Clegg et al.*, 1998], XRF (SiO_2, TiO_2, CaO, Fe_2O, Fe_2O_3, and Al_2O_3), MAAP (black carbon) and AMS (organic aerosol). (c) Black line shows volume-weighted refractive indices calculated from aerosol mass, density, and refractive index values, with organic aerosol assumed to have $k = 0$. Brown line shows the same calculation with the k for organic aerosol determined from OA absorption at 365 nm, as described in the text. (d) Dry aerosol extinction at 365 nm measured by NOAA BBCES (purple line) with light purple shading to show 4% uncertainty. Calculated aerosol optical extinction using size distributions and refractive indices, with organic aerosol assumed to have $k = 0$ (black line) and OA absorption at 365 nm (brown line). Gray shading shows uncertainty determined using Monte Carlo method (see supporting information). (e) Correlation plot for measured and calculated dry aerosol extinction at 365 nm. Linear fit (thick black line) and one-to-one line (thin black line) are shown.

©2015. American Geophysical Union. All Rights Reserved.

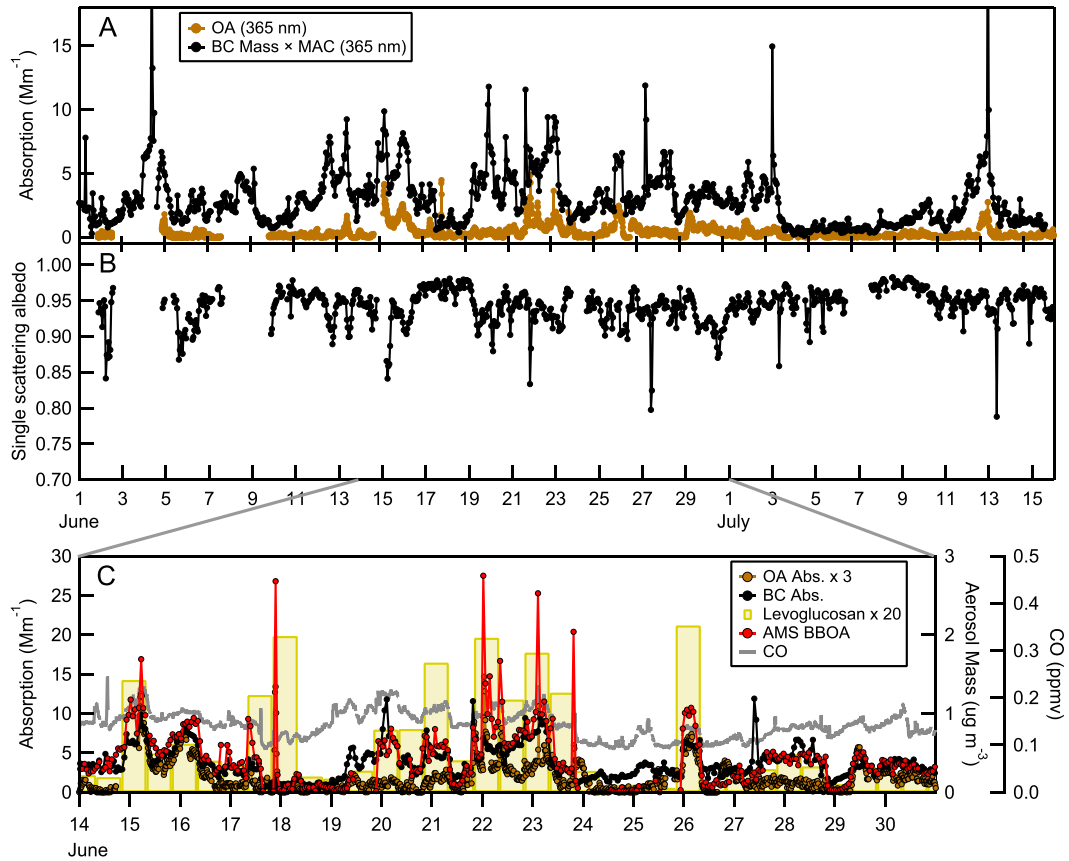

Figure 2. (a) OA and black carbon absorption at 365 nm. Black carbon absorption determined from black carbon mass and MAC = 7.5 m^2 g^{-1} at 550 nm extrapolated with an AAE of 1.0 [*Bond et al.*, 2013]. (b) Single-scattering albedo at 365 nm, calculated from absorption and BBCES extinction. (c) Time series showing correlation of OA and black carbon absorption at 365 nm with AMS biomass burning organic aerosol mass, levoglucosan aerosol mass, and CO.

Bond and Bergstrom [2006] with $m = 1.95 + 0.79i$ and $\rho = 1.8$ g cm^{-3}. The refractive index of organic aerosol is included using two alternate methods: (1) organic aerosol is assumed to be purely scattering, following the approach in *Hand and Kreidenweis* [2002] with $m = 1.55 + 0.00i$ and $\rho = 1.4$ g cm^{-3}; and (2) organic aerosol has $n = 1.55$ and an imaginary component determined from the UV/VIS-PILS measurement of OA. This is calculated from the measured bulk solution mass absorption efficiency $\left(\frac{\alpha(\lambda)}{\rho}\right)$, according to

$$k = \frac{\rho}{4\pi}\left(\frac{\alpha(\lambda)}{\rho}\right) \tag{2}$$

[*Sun et al.*, 2007; *Liu et al.*, 2013]. The average k value for OA during the SOAS field campaign was 0.004 ± 0.026.

Aerosol extinction at a given wavelength can be calculated using Mie theory together with the volume-weighted refractive indices and measured aerosol size distribution:

$$\alpha(\lambda) = \int_{D_{p,i}}^{D_{p,j}} \sigma_{\mathrm{Mie}}(\lambda, n, k)\ \mathrm{d}D_p \times N \tag{2}$$

where D_p is particle diameter, $\sigma_{\mathrm{Mie}}(\lambda, n, k)$ is the extinction cross section from Mie theory, and N is the total number of particles. Equation (2) was applied to the refractive indices in Figure 1c and measured size distributions to calculate aerosol extinction at 365 nm, as shown in Figure 1d.

For the calculations in this section and section 3.2, we assume that the composition does not vary systematically with aerosol diameter [*Attwood et al.*, 2014] and that the aerosol is internally or externally homogeneously mixed without lensing effects. Light absorption can be enhanced when a black carbon core is coated with a purely scattering material [*Fuller et al.*, 1999]. The absorption enhancement has been

©2015. American Geophysical Union. All Rights Reserved.

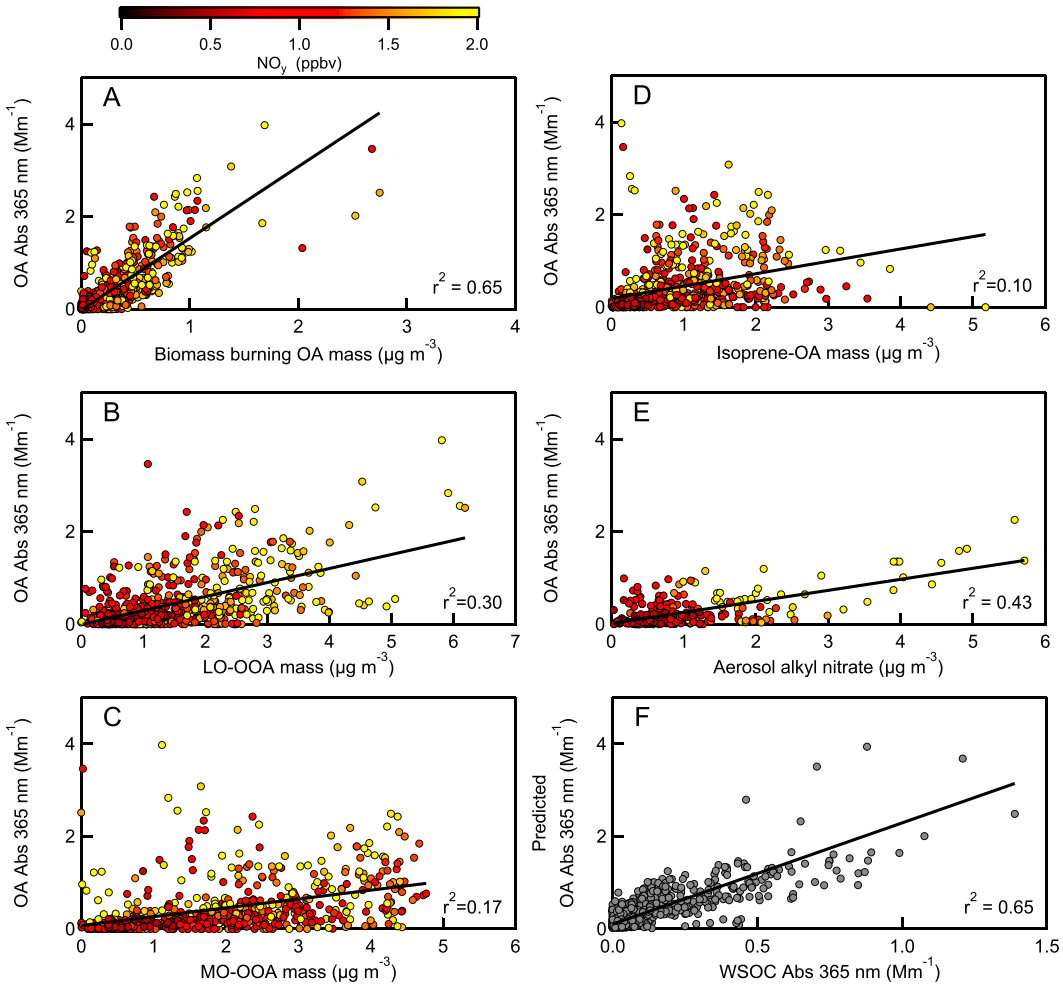

Figure 3. Correlation between OA absorption at 365 nm and the fraction of AMS organic aerosol mass that is attributed to (a) BBOA, (b) LO-OOA, (c) MO-OOA, (d) Isoprene-OA, and (e) alkyl nitrate. (f) Multiple linear regression of four AMS mass factors from equation (4). The points are colored by NO_y concentration to indicate anthropogenic influence.

calculated to be 50–100% for a purely scattering coating [*Bond et al.*, 2006] and smaller for a mildly absorbing brown carbon coating [*Lack and Cappa*, 2010]. Although we lack quantitative measurements of aerosol mixing state, we note that the observed OA was weakly absorbing and would increase black carbon absorption if it were present as a coating.

The calculated extinction value is plotted together with the BBCES measurement at 365 nm, and a correlation plot is shown in Figure 1e for the calculation that assumes that organic aerosol is purely scattering. The average uncertainty for the calculated extinction is 7.5%, as determined by Monte Carlo analysis (details in the supporting information, including uncertainties for each parameter in the calculation). An orthogonal distance regression fit gives a slope of 0.91 ± 0.01 with an intercept $-1.0 \pm 0.7\ \mathrm{Mm}^{-1}$ and $r^2 = 0.96$.

Including organic aerosol absorption with $n = 1.55$ and imaginary components determined from the UV/VIS-PILS measurement of OA gives an orthogonal distance regression fit with a slope of 0.91 ± 0.01, an intercept $-0.8 \pm 0.7\ \mathrm{Mm}^{-1}$, and $r^2 = 0.96$. This indicates that the organic aerosol absorption makes a negligible contribution to total extinction in the southeastern U. S.

3.2. Aerosol Absorption and Single-Scattering Albedo

Figure 2a compares the OA UV/VIS absorption and the absorption by black carbon. The solution-phase OA absorption must be corrected for Mie effects to determine the absorption that would be observed in the particle phase. Using measured size distributions, $\lambda = 365$ nm, $n = 1.55$, and the measured k values for OA, we

©2015. American Geophysical Union. All Rights Reserved.

determine a conversion factor of 2.00 ± 0.03, which is consistent with the result calculated in *Liu et al*. [2013] using more detailed measurements of OA and brown carbon size distributions. The black carbon absorption is calculated from the MAAP mass and a mass absorption coefficient (MAC) of 7.5 $m^2 g^{-1}$ at 550 nm [*Bond et al*., 2013] extrapolated to 365 nm with an absorption Angstrom exponent (AAE) of 1. We have not corrected the black carbon absorption for Mie effects because it is likely to be externally mixed and poorly represented by the measured size distribution. Although black carbon makes a small contribution to the total mass (3 ± 1%), it accounts for 91 ± 9% of the aerosol absorption.

The single-scattering albedo, calculated from the BBCES extinction at 365 nm and the absorption shown in Figure 2a, is determined from

$$\mathrm{SSA} = \frac{\left(\alpha_{\mathrm{extinction}} - \sum \alpha_{\mathrm{absorption}}\right)}{\alpha_{\mathrm{extinction}}} \tag{3}$$

The mean SSA value is 0.94 ± 0.02.

3.3. Contribution of Organic Aerosol Mass Factors to OA Absorption

An important scientific question with relevance to the global radiative budget is whether absorbing brown carbon aerosol is predominantly associated with primary organic aerosol and SOA from anthropogenic sources, biogenic SOA, or biomass burning OA. Figure 2c shows the time series of black and brown carbon absorption, together with levoglucosan mass, AMS BBOA mass, and CO. Black and brown carbon absorption are correlated with these biomass burning aerosol tracers. Discrete fire plumes were sampled on 15, 17, 22, and 23 June 2013, and each of these shows a corresponding peak in OA light absorption. In addition to these discrete peaks, the OA absorption tracks the longer-term variability in levoglucosan and AMS BBOA.

Figure 3 presents the correlation of OA absorption with the four AMS OA mass factors (BBOA, LO-OOA, MO-OOA, and Isoprene-OA) and aerosol alkyl nitrate. The points in each panel are colored by NO_y, to indicate anthropogenic influence. The correlation coefficients, r^2, for OA absorption with each of the OA mass factors and alkyl nitrate are 0.65, 0.30, 0.17, 0.10, and 0.43, respectively.

The four AMS OA mass factors account for the complete PM_1 organic aerosol mass within errors. A multiple linear regression of the four AMS factors gives the mass absorption coefficient (MAC) at 365 nm of each factor, with $r^2 = 0.65$:

$$\begin{aligned}\alpha_{\mathrm{absorption,\ brown\ carbon}} = {} & (1.35 \pm 0.06)\ \mathrm{m^2 g^{-1}} \times \mathrm{BBOA} \\ & + (0.033 \pm 0.016)\ \mathrm{m^2 g^{-1}} \times \mathrm{LOOOA} \\ & - (0.010 \pm 0.014)\ \mathrm{m^2 g^{-1}} \times \mathrm{MOOOA} \\ & - (0.010 \pm 0.023)\ \mathrm{m^2 g^{-1}} \times \mathrm{Isoprene\text{-}OA} \\ & + (0.018 \pm 0.029)\ \mathrm{Mm^{-1}}\end{aligned} \tag{4}$$

The negative coefficients for MO-OOA and Isoprene-OA are not significantly different from zero. The MAC value for BBOA is similar to values previously reported for biomass burning, which include 2.5 $m^2 g^{-1}$ and 1.4 $m^2 g^{-1}$ for organic matter at 350 and 400 nm [*Kirchstetter et al*., 2004] (assuming a conversion of 2.0 from OC to OA) and 0.82 ± 0.43 $m^2 g^{-1}$ for organic matter at 404 nm [*Lack et al*., 2012]. The four AMS OA mass factors had similar average size distributions, with mode diameters consistent within 15% for tracer ions corresponding to each factor, so differing Mie effects are neglected in the multiple linear regression.

Multiplying by the mean mass concentration of each organic aerosol component gives their contribution to absorption during June–July 2013, as shown in Figure 4a. BBOA, LO-OOA, MO-OOA, and Isoprene-OA contributed 8.7%, 0.7%, −0.3%, and −0.4% of the total mean aerosol absorption, respectively. A recent laboratory chamber study suggested that aerosol generated from isoprene epoxydiol uptake under dry and acidic conditions could be a potentially significant source of brown carbon in the southeastern U.S. [*Lin et al*., 2014]. However, our results indicate that the brown carbon absorption in this region is weakly correlated with isoprene SOA. One explanation is that some strongly absorbing chromophores exist within Isoprene-OA, but they do not dominate the mass. Further studies are needed to resolve this.

Although biomass burning aerosol contributes the majority of brown carbon absorption, it is not a major contributor to aerosol mass in this study (Figure 4b). The mean mass fraction of BBOA to total OA was

©2015. American Geophysical Union. All Rights Reserved.

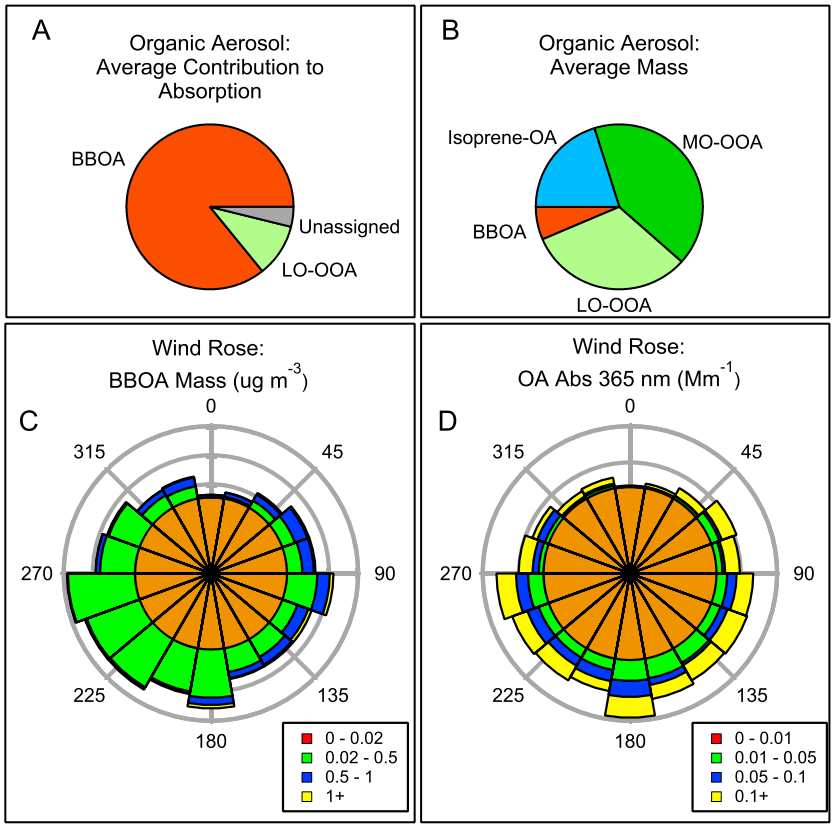

Figure 4. Fractional contribution of AMS organic aerosol mass factors during 1 June to 15 July 2013 to (a) OA absorption and (b) mass. (c) Wind roses showing frequency distribution of biomass burning organic aerosol mass with legend indicating color code for each size bin in $\mu g\ m^{-3}$ and (d) OA absorption at 365 nm with legend indicating color code for each size bin in Mm^{-1}.

0.06 ± 0.07 during the periods when brown carbon absorption was measured, although it exceeded 0.5 during plume events. In order to determine if the biomass burning aerosol mass and OA absorption had a local source or were distributed regionally, we plotted wind roses examining biomass burning aerosol as a function of wind speed and direction (Figures 4c and 4d). Neither the biomass burning markers nor the brown carbon absorption was associated with systematic transport from a particular direction. This suggests a regional background that is not associated with discrete, repeatable upwind sources.

3.4. Seasonal Changes in Organic Aerosol Mass Concentrations

The MAC coefficients determined above are intrinsic characteristics of the aerosol sampled during SOAS. However, the fractional contribution of biomass burning brown carbon to the total aerosol absorption in this analysis is specific to June–July in the southeastern U.S. and will be greater during winter and spring when biomass burning emissions are greater [*Zheng et al.*, 2002; *Tian et al.*, 2009; *Zhang et al.*, 2010]. Using chemical tracers, *Zhang et al.* [2010] estimate biomass burning aerosol concentrations in the southeastern U.S. of $0.4 \pm 0.2\ \mu g\ m^{-3}$ during summer (June-July-August) and $3.2 \pm 1.7\ \mu g\ m^{-3}$ during winter (December-January-February), indicating that brown carbon absorption by biomass burning aerosol is 8 times greater in winter than in summer. Apportionment of $PM_{2.5}$ organic carbon at the Centreville SEARCH site using chemical tracers concluded that the wood combustion mass factor increased by 8.7 times and 5.4 times in October and January compared to July [*Zheng et al.*, 2002], while chemical transport modeling for Georgia determined that biomass burning emissions contribute 10 times more mass during January compared to July [*Tian et al.*, 2009].

The LO-OOA, MO-OOA, and Isoprene-OA mass factors will also vary seasonally, as concentrations of VOCs and oxidants change [*Hagerman et al.*, 1997; *Xu et al.*, 2014]. Additionally, aerosol pH and water content will vary

©2015. American Geophysical Union. All Rights Reserved.

seasonally, which may affect biogenic OA formation and properties. The seasonal variation in these SOA sources and their contribution to brown carbon absorption is difficult to estimate without a mechanistic understanding of their source chemistry. The evidence that biomass burning aerosol makes the dominant contribution to brown carbon absorption during June and July, and that its mass concentrations are 5–10 times greater during fall and winter when brown carbon is absorption is greater [*Hecobian et al*., 2010; *Verma et al*., 2014], indicates that it could be the major source of brown carbon absorption in the southeastern U.S. on an annual average.

4. Conclusions

Measured aerosol optical extinction and extinction calculated from composition, size distribution, and Mie theory shows agreement within experimental uncertainties. In summer 2013, aerosol optical extinction in the southeastern U.S. was dominated by scattering, with calculated single-scattering albedo values of 0.94 ± 0.02. Brown carbon absorption decreases with increasing wavelength toward the peak of the solar spectrum, which suggests that it makes a small contribution to aerosol single-scattering albedo at midvisible wavelengths. Black carbon aerosol produced $91 \pm 9\%$ of the total carbonaceous aerosol absorption, while organic brown carbon aerosol contributed $9 \pm 9\%$ at 365 nm. Although this value will vary with season, geography, and emission sources, we note that it is consistent with measurements showing that brown carbon contributed approximately 10% at 405 nm for two regions in California during summer 2010 [*Cappa et al*., 2012]. In contrast, other studies have shown brown carbon contributions of 20–40% at 350 nm using measurements at urban and rural sites in Georgia [*Liu et al*., 2013], 28% at 440 nm using aerosol optical depth observations in California [*Bahadur et al*., 2012], and ~30% at 370 nm using source apportionment in Xianghe, China [*Yang et al*., 2009].

Absorption by organic aerosol was associated primarily with markers of biomass burning. It is more weakly correlated with biogenic VOC emissions and biogenic secondary organic aerosol. Previous studies have shown that biomass burning aerosol mass concentrations in the southeastern U.S. are lowest during the summer, and 8–10 times greater during fall and winter, suggesting that brown carbon absorption may be much more important in the winter.

Acknowledgments
Data from SOAS are publicly available at http://www.esrl.noaa.gov/csd/projects/senex/. We thank Ann Marie Carlton and the SOAS organizers for coordinating the SOAS field site, and SEARCH for hosting it. We thank Stuart McKeen for U.S. EPA National Emission Inventory data. We thank Abigail Koss, Jessica Gilman, Brian Lerner, Joost de Gouw, Kevin Olson, and Allen Goldstein for GC-MS data. R.A.W., A.R.A., C.A.B., and S.S.B. acknowledge support from the NOAA Atmospheric Chemistry, Carbon Cycle and Climate Program (AC4). W.W. H., B.B.P., and J.L.J. acknowledge support from NSF AGS-1243354, NOAA NA13OAR4310063, and DOE (BER/ASR) DE-SC0011105. E.A.S. acknowledges support from EPA STAR-83540101.

The Editor thanks two anonymous reviewers for assistance in evaluating this paper.

References

Andreae, M. O., and P. J. Crutzen (1997), Atmospheric aerosols: Biogeochemical sources and role in atmospheric chemistry, *Science*, *276*(5315), 1052–1058.

Andreae, M. O., and A. Gelencsér (2006), Black carbon or brown carbon? The nature of light-absorbing carbonaceous aerosols, *Atmos. Chem. Phys.*, *6*, 3131–3148.

Attwood, A. R., et al. (2014), Trends in sulfate and organic aerosol mass in the Southeast U.S.: Impact on aerosol optical depth and radiative forcing, *Geophys. Res. Lett.*, *41*, 7701–7709, doi:10.1002/2014GL061669.

Bahadur, R., P. S. Praveen, Y. Y. Xu, and V. Ramanathan (2012), Solar absorption by elemental and brown carbon determined from spectral observations, *Proc. Natl. Acad. Sci. U.S.A.*, *109*, 17,366–17,371.

Ball, S. M., J. M. Langridge, and R. L. Jones (2004), Broadband cavity enhanced absorption spectroscopy using light emitting diodes, *Chem. Phys. Lett.*, *398*, 68–74.

Bond, T. C. (2001), Spectral dependence of visible light absorption by carbonaceous particles emitted from coal combustion, *Geophys. Res. Lett.*, *28*(21), 4075–4078, doi:10.1029/2001GL013652.

Bond, T. C., and R. W. Bergstrom (2006), Light absorption by carbonaceous particles: An investigative review, *Aerosol Sci. Technol.*, *40*, 27–67.

Bond, T. C., G. Habib, and R. W. Bergstrom (2006), Limitations in the enhancement of visible light absorption due to mixing state, *J. Geophys. Res.*, *111*, doi:10.1029/2006JD007315.

Bond, T. C., et al. (2013), Bounding the role of black carbon in the climate system: A scientific assessment, *J. Geophys. Res. Atmos.*, *118*, doi:10.1002/jgrd.50171.

Bones, D. L., D. K. Henricksen, S. A. Mang, M. Gonsior, A. P. Bateman, T. B. Nguyen, W. J. Cooper, and S. A. Nizkorodov (2010), Appearance of strong absorbers and fluorophores in limonene-O_3 secondary organic aerosol due to NH_4^+-mediated chemical aging over long time scales, *J. Geophys. Res.*, *115*, doi:10.1029/2009JD012864.

Canagaratna, M. R., et al. (2007), Chemical and microphysical characterization of ambient aerosols with the aerodyne aerosol mass spectrometer, *Mass Spectrom. Rev.*, *26*, 185–222.

Cappa, C. D., et al. (2012), Radiative absorption enhancements due to the mixing state of atmospheric black carbon, *Science*, *337*, 1078–1081.

Chen, Y., and T. C. Bond (2010), Light absorption by organic carbon from wood combustion, *Atmos. Chem. Phys.*, *10*, 1773–1787.

Chung, C. E., V. Ramanathan, and D. Decremer (2012), Observationally constrained estimates of carbonaceous aerosol radiative forcing, *Proc. Natl. Acad. Sci. U.S.A.*, *109*, 11,624–11,629.

Clegg, S. L., P. Brimblecombe, and A. S. Wexler (1998), Thermodynamic model of the system H^+-NH_4^+-Na^+-SO_4^{2-}-NO_3^--Cl^--H_2O at 298.15 K, *J. Chem. Phys. A*, *102*(12), 2155–2171.

DeCarlo, P. F., et al. (2006), Field-deployable, high-resolution, time-of-flight aerosol mass spectrometer, *Anal. Chem.*, *78*, 8281–8289.

©2015. American Geophysical Union. All Rights Reserved.

Edgerton, E. S., B. E. Hartsell, R. D. Saylor, J. J. Jansen, D. A. Hansen, and G. M. Hidy (2005), The Southeastern Aerosol Research and Characterization Study: Part II. Filter-based measurements of fine and coarse particulate matter mass and composition, *J. Air Waste Manage.*, *55*, 1527–1542.

Edgerton, E. S., B. E. Hartsell, R. D. Saylor, J. J. Jansen, D. A. Hansen, and G. M. Hidy (2006), The Southeastern Aerosol Research and Characterization Study, part 3: Continuous measurements of fine particulate matter mass and composition, *J. Air Waste Manage.*, *56*, 1325–1341.

Fiedler, S. E., A. Hese, and A. A. Ruth (2003), Incoherent broad-band cavity-enhanced absorption spectroscopy, *Chem. Phys. Lett.*, *371*(3–4), 284–294.

Flores, J. M., R. A. Washenfelder, G. Adler, H. J. Lee, L. Segev, J. Laskin, A. Laskin, S. A. Nizkorodov, S. S. Brown, and Y. Rudich (2014), Complex refractive indices in the near-ultraviolet spectral region of biogenic secondary organic aerosol aged with ammonia, *Phys. Chem. Chem. Phys.*, *16*, 10,629–10,642.

Fuller, K. A., W. C. Malm, and S. M. Kreidenweis (1999), Effects of mixing on extinction by carbonaceous particles, *J. Geophys. Res.*, *104*, 15,491–15,954.

Gelencser, A., A. Hoffer, G. Kiss, E. Tombacz, R. Kurdi, and L. Bencze (2003), In-situ formation of light-absorbing organic matter in cloud water, *J. Atmos. Chem.*, *45*(1), 25–33.

Guenther, A. B., X. Jiang, C. L. Heald, T. Sakulyanontvittaya, T. Duhl, L. K. Emmons, and X. Wang (2012), The Model of Emissions of Gases and Aerosols from Nature version 2.1 (MEGAN2.1): An extended and updated framework for modeling biogenic emissions, *Geosci. Model Dev.*, *5*, 1471–1492.

Hagerman, L. M., V. P. Aneja, and W. A. Lonneman (1997), Characterization of non-methane hydrocarbons in the rural southeast United States, *Atmos. Environ.*, *31*(23), 4017–4038.

Hand, J. L., and S. M. Kreidenweis (2002), A new method for retrieving particle refractive index and effective density from aerosol size distribution data, *Aerosol Sci. Technol.*, *36*(10), 1012–1026.

Hansen, D. A., E. S. Edgerton, B. E. Hartsell, J. J. Jansen, N. Kandasamy, G. M. Hidy, and C. L. Blanchard (2003), The Southeastern Aerosol Research and Characterization Study: Part 1—Overview, *J. Air Waste Manage.*, *53*(12), 1460–1471.

Hecobian, A., X. Zhang, M. Zheng, N. Frank, E. S. Edgerton, and R. J. Weber (2010), Water-soluble organic aerosol material and the light-absorption characteristics of aqueous extracts measured over the Southeastern United States, *Atmos. Chem. Phys.*, *10*, 5965–5977.

Hoffer, A., G. Kiss, M. Blazso, and A. Gelencser (2004), Chemical characterization of humic-like substances (HULIS) formed from a lignin-type precursor in model cloud water, *Geophys. Res. Lett.*, *31*, doi:10.1029/2003GL018962.

Jacobson, M. Z. (1999), Isolating nitrated and aromatic aerosols and nitrated aromatic gases as sources of ultraviolet light absorption, *J. Geophys. Res.*, *104*(D3), 3527–3542, doi:10.1029/1998JD100054.

Kirchstetter, T. W., T. Novakov, and P. V. Hobbs (2004), Evidence that the spectral dependence of light absorption by aerosols is affected by organic carbon, *J. Geophys. Res.*, *109*, doi:10.1029/2004JD004999.

Lack, D. A., and C. D. Cappa (2010), Impact of brown and clear carbon on light absorption enhancement, single scatter albedo and absorption wavelength dependence of black carbon, *Atmos. Chem. Phys.*, *10*, 4207–4220.

Lack, D. A., J. M. Langridge, R. Bahreini, C. D. Cappa, A. M. Middlebrook, and J. P. Schwarz (2012), Brown carbon and internal mixing in biomass burning particles, *Proc. Natl. Acad. Sci. U.S.A.*, *109*, 14,802–14,807.

Limbeck, A., M. Kulmala, and H. Puxbaum (2003), Secondary organic aerosol formation in the atmosphere via heterogeneous reaction of gaseous isoprene on acidic particles, *Geophys. Res. Lett.*, *30*(19), doi:10.1029/2003GL017738.

Lin, Y.-H., S. H. Budisulistiorini, K. Chu, R. A. Siejack, H. Zhang, M. Riva, Z. Zhang, A. Gold, K. E. Kautzman, and J. D. Surratt (2014), Light-absorbing oligomer formation in secondary organic aerosol from reactive uptake of isoprene epoxydiols, *Environ. Sci. Technol.*, *48*(20), 2,012,012–2,012,021.

Liu, J., M. Bergin, H. Guo, L. King, N. Kotra, E. Edgerton, and R. J. Weber (2013), Size-resolved measurements of brown carbon in water and methanol extracts and estimates of their contribution to ambient fine-particle light absorption, *Atmos. Chem. Phys.*, *13*, 12,389–12,404.

Mohr, C., et al. (2013), Contribution of nitrated phenols to wood burning brown carbon light absorption in Detling, United Kingdom during winter time, *Environ. Sci. Technol.*, *47*, 6316–6324.

Nolte, C. G., J. J. Schauer, G. R. Cass, and B. R. T. Simoneit (2002), Trimethylsilyl derivatives of organic compounds in source samples and in atmospheric fine particulate matter, *Environ. Sci. Technol.*, *36*(20), 4273–4281.

Noziere, B., and W. Esteve (2005), Organic reactions increasing the absorption index of atmospheric sulfuric acid aerosols, *Geophys. Res. Lett.*, *32*, doi:10.1029/2004GL021942.

Noziere, B., and W. Esteve (2007), Light-absorbing aldol condensation products in acidic aerosols: Spectra, kinetics, and contribution to the absorption index, *Atmos. Environ.*, *41*, 1150–1163.

Ouimette, J. R., and R. C. Flagan (1982), The extinction coefficient of multicomponent aerosols, *Atmos. Environ.*, *16*(10), 2405–2419.

Petzold, A., H. Kramer, and M. Schonlinner (2002), Continuous measurement of atmospheric black carbon using a multi-angle absorption photometer, *Environ. Sci. Pollut. Res.*, (Special Issue 4), 78–82.

Pitts, J. N., K. A. Vancauwenberghe, D. Grosjean, J. P. Schmid, D. R. Fitz, W. L. Belser, G. B. Knudson, and P. M. Hynds (1978), Atmospheric reactions of polycyclic aromatic hydrocarbons—Facile formation of mutagenic nitro-derivatives, *Science*, *202*(4367), 515–519.

Rincon, A. G., M. I. Guzman, M. R. Hoffmann, and A. J. Colussi (2009), Optical absorptivity versus molecular composition of model organic aerosol matter, *J. Phys. Chem. A*, *113*, 10,512–10,520.

Rincon, A. G., M. I. Guzman, M. R. Hoffmann, and A. J. Colussi (2010), Thermochromism of model organic aerosol matter, *J. Phys. Chem. Lett.*, *1*, 368–373.

Rollins, A. W., J. D. Smith, K. R. Wilson, and R. C. Cohen (2010), Real time in situ detection of organic nitrates in atmospheric aerosols, *Environ. Sci. Technol.*, *44*, 5540–5545.

Rumsey, I. C., et al. (2014), An assessment of the performance of the Monitor for AeRosols and GAses in ambient air (MARGA): A semi-continuous method for soluble compounds, *Atmos. Chem. Phys.*, *14*, 5639–5658.

Sareen, N., A. N. Schwier, E. L. Shapiro, D. Mitroo, and V. F. McNeill (2010), Secondary organic material formed by methylglyoxal in aqueous aerosol mimics, *Atmos. Chem. Phys.*, *10*, 997–1016.

Slanina, J., H. M. ten Brink, R. P. Otjes, A. Even, P. Jongejan, A. Khlystov, A. Waijers-Ijpelaan, and M. Hu (2001), The continuous analysis of nitrate and ammonium in aerosols by the steam jet aerosol collector (SJAC): Extension and validation of the methodology, *Atmos. Environ.*, *35*(13), 2319–2330.

Solomon, S., D. Qin, M. Manning, M. Marquis, K. Averyt, M. M. B. Tignor, and H. L. Miller (Eds.) (2007), *Climate Change 2007: The Physical Science Basis*, Cambridge Univ. Press, Cambridge, U. K.

Sun, H. L., L. Biedermann, and T. C. Bond (2007), Color of brown carbon: A model for ultraviolet and visible light absorption by organic carbon aerosol, *Geophys. Res. Lett.*, *34*, doi:10.1029/2007GL029797.

©2015. American Geophysical Union. All Rights Reserved.

Thalman, R., and R. Volkamer (2010), Inherent calibration of a blue LED-CE-DOAS instrument to measure iodine oxide, glyoxal, methyl glyoxal, nitrogen dioxide, water vapour and aerosol extinction in open cavity mode, *Atmos. Meas. Tech.*, *3*, 1797–1814.

Tian, D., Y. T. Hu, Y. H. Wang, J. W. Boylan, M. Zheng, and A. G. Russell (2009), Assessment of biomass burning emissions and their impacts on urban and regional PM2.5: A Georgia case study, *Environ. Sci. Technol.*, *43*, 299–305.

Ulbrich, I. M., M. R. Canagaratna, Q. Zhang, D. R. Worsnop, and J. L. Jimenez (2009), Interpretation of organic components from positive matrix factorization of aerosol mass spectrometric data, *Atmos. Chem. Phys.*, *9*, 2891–2918.

Updyke, K. M., T. B. Nguyen, and S. A. Nizkorodov (2012), Formation of brown carbon via reactions of ammonia with secondary organic aerosols from biogenic and anthropogenic precursors, *Atmos. Environ.*, *63*, 22–31.

Varma, R. M., D. S. Venables, A. A. Ruth, U. Heitmann, E. Schlosser, and S. Dixneuf (2009), Long optical cavities for open-path monitoring of atmospheric trace gases and aerosol extinction, *Appl. Opt.*, *48*(4), B159–B171.

Varma, R. M., et al. (2013), Light extinction by secondary organic aerosol: An intercomparison of three broadband cavity spectrometers, *Atmos. Meas. Tech.*, *6*, 3115–3130.

Venables, D. S., T. Gherman, J. Orphal, J. C. Wenger, and A. A. Ruth (2006), High sensitivity in situ monitoring of NO_3 in an atmospheric simulation chamber using incoherent broadband cavity-enhanced absorption spectroscopy, *Environ. Sci. Technol.*, *40*, 6758–6763.

Verma, V., T. Fang, H. Guo, L. King, J. T. Bates, R. E. Peltier, E. Edgerton, A. G. Russell, and R. J. Weber (2014), Reactive oxygen species associated with water-soluble $PM_{2.5}$ in the southeastern United States: spatiotemporal trends and source apportionment, *Atmos. Chem. Phys.*, *14*, 12,915–12,930.

Washenfelder, R. A., A. O. Langford, H. Fuchs, and S. S. Brown (2008), Measurement of glyoxal using an incoherent broadband cavity enhanced absorption spectrometer, *Atmos. Chem. Phys.*, *8*, 7779–7793.

Washenfelder, R. A., et al. (2011), The glyoxal budget and its contribution to organic aerosol for Los Angeles, California during CalNex 2010, *J. Geophys. Res.*, *116*, doi:10.1029/2011JD016314.

Washenfelder, R. A., J. M. Flores, C. A. Brock, S. S. Brown, and Y. Rudich (2013), Broadband measurements of aerosol extinction in the ultraviolet spectral region, *Atmos. Meas. Tech.*, *6*, 861–877.

Xu, L., et al. (2014), Effects of anthropogenic emissions on aerosol formation from isoprene and monoterpenes in the southeastern United States, *Proc. Natl. Acad. Sci. U.S.A.*, *112*, 37–42, doi:10.1073/pnas.1417609112.

Yang, M., S. G. Howell, J. Zhuang, and B. J. Huebert (2009), Attribution of aerosol light absorption to black carbon, brown carbon, and dust in China—Interpretations of atmospheric measurements during EAST-AIRE, *Atmos. Chem. Phys.*, *9*, 2035–2050.

Zhang, X., A. Hecobian, M. Zheng, N. H. Frank, and R. J. Weber (2010), Biomass burning impact on $PM_{2.5}$ over the southeastern US during 2007: Integrating chemically speciated FRM filter measurements, MODIS fire counts and PMF analysis, *Atmos. Chem. Phys.*, *10*, 6839–6853.

Zhang, X. L., Y. H. Lin, J. D. Surratt, P. Zotter, A. S. H. Prevot, and R. J. Weber (2011), Light-absorbing soluble organic aerosol in Los Angeles and Atlanta: A contrast in secondary organic aerosol, *Geophys. Res. Lett.*, *38*, doi:10.1029/2011GL049385.

Zhang, X. L., Y. H. Lin, J. D. Surratt, and R. J. Weber (2013), Sources, composition and absorption Angstrom exponent of light-absorbing organic components in aerosol extracts from the Los Angeles Basin, *Environ. Sci. Technol.*, *47*, 3685–3693.

Zheng, M., G. R. Cass, J. J. Schauer, and E. S. Edgerton (2002), Source apportionment of PM2.5 in the southeastern United States using solvent-extractable organic compounds as tracers, *Environ. Sci. Technol.*, *36*(11), 2361–2371.

©2015. American Geophysical Union. All Rights Reserved.